Nanocellulose−Zeolite Composite Films for Odor Elimination

Neda Keshavarzi,[†] Farshid Mashayekhy Rad,[‡] Amber Mace,[†] Farhan Ansari,[||] Farid Akhtar,[§] Ulrika Nilsson,[‡] Lars Berglund,[||] and Lennart Bergström*[,†]

[†]Department of Materials and Environmental Chemistry, Stockholm University, SE-106 91 Stockholm, Sweden
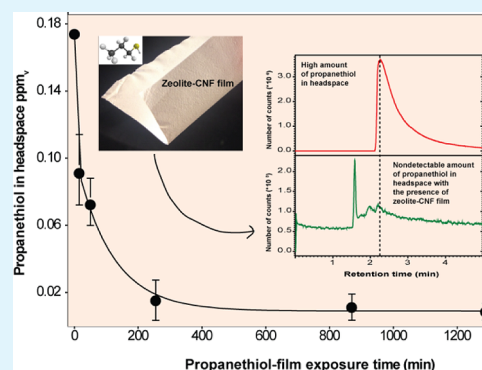[‡]Department of Analytical Chemistry, Stockholm University, SE-106 91 Stockholm, Sweden
[§]Division of Materials Science, Luleå University of Technology, Luleå, SE- 97187 Sweden
[||]Wallenberg Wood Science Center, Royal Institute of Technology, KTH, SE-10044 Stockholm, Sweden

Ⓢ Supporting Information

ABSTRACT: Free standing and strong odor-removing composite films of cellulose nanofibrils (CNF) with a high content of nanoporous zeolite adsorbents have been colloidally processed. Thermogravimetric desorption analysis (TGA) and infrared spectroscopy combined with computational simulations showed that commercially available silicalite-1 and ZSM-5 have a high affinity and uptake of volatile odors like ethanethiol and propanethiol, also in the presence of water. The simulations showed that propanethiol has a higher affinity, up to 16%, to the two zeolites compared with ethanethiol. Highly flexible and strong free-standing zeolite−CNF films with an adsorbent loading of 89 w/w% have been produced by Ca-induced gelation and vacuum filtration. The CNF-network controls the strength of the composite films and 100 μm thick zeolite−CNF films with a CNF content of less than 10 vol % displayed a tensile strength approaching 10 MPa. Headspace solid phase microextraction (SPME) coupled to gas chromatography−mass spectroscopy

(GC/MS) analysis showed that the CNF−zeolite films can eliminate the volatile thiol-based odors to concentrations below the detection ability of the human olfactory system. Odor removing zeolite−cellulose nanofibril films could enable improved transport and storage of fruits and vegetables rich in odors, for example, onion and the tasty but foul-smelling South-East Asian Durian fruit.

KEYWORDS: nanocellulose, zeolite, odor, composite, strength, colloidal processing, packaging

INTRODUCTION

Volatile sulfur-containing organic compounds are the main cause of the fetid smell emanating from decomposition products and some fruits and vegetables, for example, garlic, leek, onion, and the tasty durian fruit.[1−4] Indeed, the smell of durian fruit is considered to be so foul that it is not permitted on the Singapore subway system and many airlines.[5] Packaging and storage of odorant food products is challenging, and the concentration of odors may reach unbearable levels for the human olfactory system. Urbanization and growing global transport of food products increase the demand for efficient odor eliminating strategies.

Strategies for odor elimination include chemical reactions, absorption, or adsorption, and combinations of these approaches.[6,7] Packaging solutions for odor removal that utilizes commercially available adsorbents, for example, zeolites, activated alumina, activated carbon, silica, sodium bicarbonate, and titanium oxide have been developed and reported in the scientific and patent literature.[8−17] Previous studies have shown that alumina and silica nanoparticles modified by different metal ions can be introduced in packaging materials and adsorb, for example, mercaptans and sulfur-containing compounds.[11,12]

Activated carbon have been introduced in paper laminates for wrapping and packaging of odorous food products.[13] However, activated carbons are often avoided in packaging because of the unattractive, black color and sometimes weak deodorizing ability in the presence of moisture.[11] Zeolite molecular sieves are interesting adsorbents, which are widely used for gas and liquid separation.[18,19] Sulfur-containing volatile compounds have been removed by FAU-type (X and Y) and MFI-type (ZSM-5) zeolites and also metal organic frameworks.[9,20−23] Zeolites of the Faujasite type have been incorporated in packaging films for the removal of byproducts from oxygen scavenging processes in food products.[14] Zeolites of FAU-type and MFI-type have three-dimensional pore systems that can accommodate a sphere with maximum diameter of 11.2 and 6.36 Å and have an accessible volume of 3956 and 511 Å^3 for water molecules, respectively.[24] Zeolites with a high content of SiO$_2$ and medium to large pore diameter (5.5−6.0 Å) have previously been identified as good candidates for uptake of
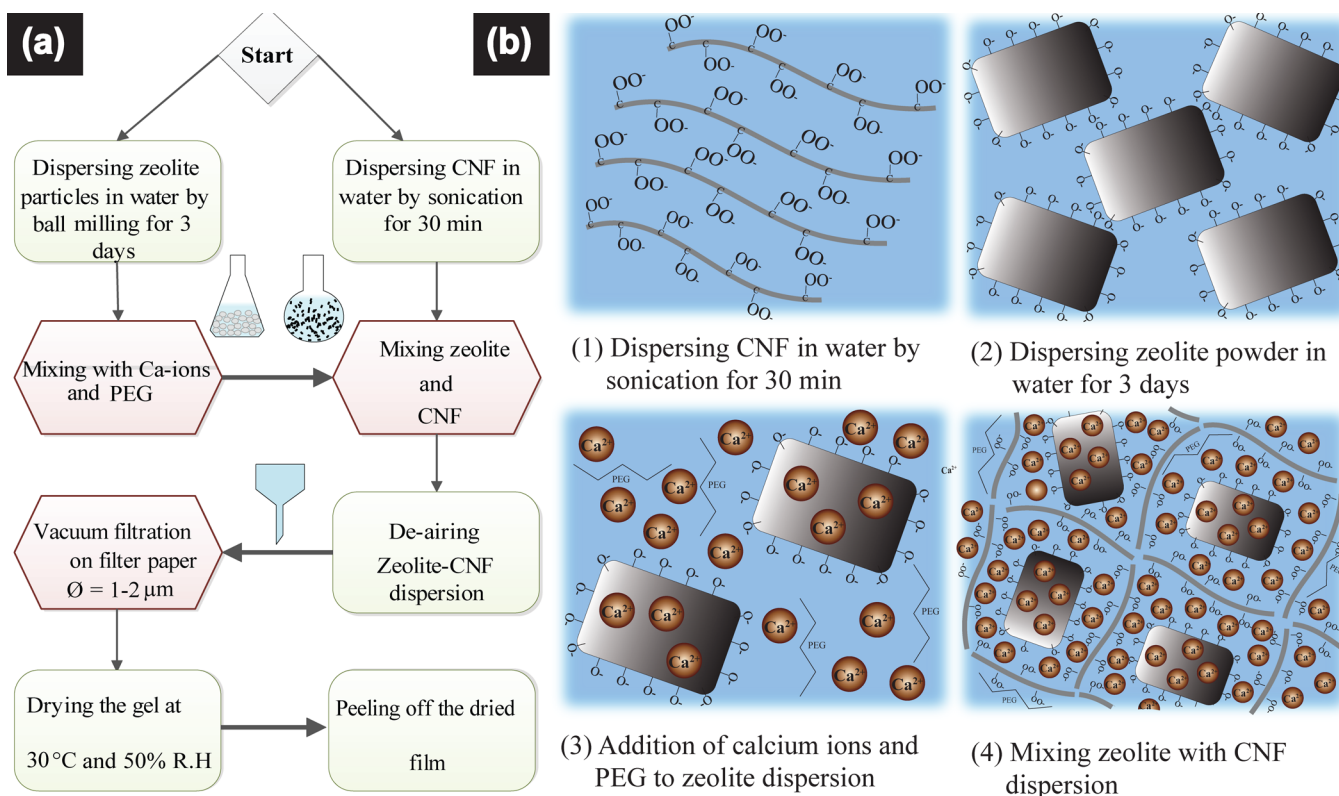
Figure 1. Preparation of dispersions and films of cellulose nanofibrils and zeolites: (a) Flowchart summarizing the preparation steps of zeolite−CNF films. (b) Schematic illustrations (1−4) showing the surface characteristics of CNF and zeolite particles and the formation of a hybrid network in aqueous solution.

sulfur and nitrogen containing volatile compounds.[15] Composites of zeolites with cellulose have been prepared by deposition of zeolite particles onto the cellulose fibers[25] and zeolite−cellulose laminates and composites for efficient removal of NH₃ and NO₂ gases have also been produced by in situ synthesis of zeolite crystals on cellulose.[17] Polymer-based composite films are extensively used as gas barriers and Huang et al. studied the effect of zeolite beta particles on the gas barrier properties of polyethylene-based composite films.[16] However, introducing microporous adsorbents in polymer films can result in pore blockage and slow diffusion.[26−28] Reducing the dimensions of cellulose from fibers to nanosized crystals or fibrils offer the possibility to produce stronger films and coatings[29] and to maximize the amount of active component (the zeolite particles) while obtaining a sufficient mechanical strength. Cellulose nanofibrils (CNF) has an impressive stiffness of around 140 GPa[29,30] and previous work has shown that mechanically strong and transparent films can be produced.[31]

This work aims to identify suitable low-cost microporous adsorbents and to prepare zeolite−cellulose nanofibril films with a high amount of the active component that can be used as odor-removing materials. We show that composites of zeolite−cellulose nanofibril films are suitable for capturing highly volatile sulfur containing compounds emanating, for example, from the foul-smelling Durian fruit. Composite films of selected zeolites and negatively charged cellulose nanofibrils[31] have been prepared by a colloidal processing approach involving Ca-ion induced gelation and vacuum filtration. The uptake properties of the zeolite powders and the flexibility, mechanical properties and porosity of the zeolite−cellulose nanofibril composite films have been determined by a combination of TGA, GC-MC

simulations, DFT calculation, FT-IR spectroscopy, SEM, mechanical and N₂ adsorption measurements. The interactions between the thiols and zeolites have been simulated and the competition between water and thiols was analyzed. The mechanical properties of the zeolite−cellulose composite films were related to structure and composition. The removal efficiency for thiols of low molecular weights (ethanethiol and propanethiol) was analyzed using GC-head space measurements and a sniff test was designed to verify that the zeolite−nanocellulose composites could reduce the thiol concentration below the threshold that can be detected by the human olfactory system.

■ MATERIALS AND METHODS

Materials. The zeolite powders of different type; silicalite-1 powder (MFI type, Si/Al = 1200, particle size ~3−5 μm, Sud-Chemie AG, Bruckmühl, Germany), ZSM-5 powder (MFI type, cation = ammonium, Si/Al = 140, particle size ~0.5−1.5 μm, Zeolyst Int. USA), zeolite beta powder (BEA type, cation = hydrogen, Si/Al = 180, particle size ~1.5−2.0 μm, Zeolyst Int. USA), zeolite Y powder (FAU type, cation = hydrogen, Si/Al = 15, particle size ~0.5−1.5 μm, Zeolyst Int. USA), and mordenite powder (MOR type, cation = hydrogen, Si/Al = 45, particle size ~1.5−2.0 μm, Zeolyst Int. USA) were used as-received. The two low molecular weight thiols, ethanethiol (T_b = 35 °C, Sigma-Aldrich Chemie GmbH, Germany) and propanethiol (T_b = 67 °C, Sigma-Aldrich Chemie GmbH, Germany) were used as the target odors. Cellulose nanofibrils (CNF) with a surface charge density of 600 μeq/g used in this work were prepared by TEMPO oxidation of wood fiber at the Wallenberg wood science center according to the procedure previously reported by Saito et al.[32] CaCl₂ (Merck, Darmstad, Germany) and polyethylene glycol (PEG, Sigma-Aldrich Chemie GmbH, Germany, M_w = 8000 g/mol) were used as-received.

Preparation of Dispersions and Films. The steps for fabrication of zeolite−CNF films are shown in the flowchart in Figure 1a. Cellulose nanofibrils (CNF) dispersions with a concentration of 0.05 wt % were prepared by dispersing 5 g of 1 wt % TEMPO-oxidized cellulose nanofibrils (CNF) in 100 mL of Millipore water by stirring for 15 min and sonication in an ultrasonic bath for 30 min. The three selected zeolite powders: zeolite Y, ZSM-5, and silicalite-1, were dispersed in water and deagglomerated for 3 days by mild ball-milling in rotating polyethylene containers using spherical alumina balls of 6 mm in diameter. Dilute aqueous dispersions of the deagglomerated zeolite particles with a concentration of 0.5−2 wt % and pH values ranging from 4.0 to 6.0 were prepared and mixed with 0.01 wt % polyethylene glycol and 13 mmol/L of CaCl$_2$ (Figure 1b). Homogeneous composite dispersions of zeolite and CNF were obtained by mixing the CNF dispersion (0.05 wt %) with a zeolite dispersion (0.5 wt %) that were sonicated and deaired (Figure 1b). Free standing films were formed by vacuum filtration of the Ca-ion cross-linked zeolite−CNF dispersion using filter papers with pore diameter of 1−2 μm (Grade 120H, Munktell Filter AB, Sweden). A combination of calcium gelation and vacuum filtration method results in strong cellulose network containing zeolite particles as reported previously.[33] Most of the water was removed by treating the films in a climate chamber (KBF 115, Binder, Germany) at 30 °C and 50% relative humidity (RH) for 24 h. Zeolite contents of zeolite−CNF free-standing films are reported based on weight percentage of dry constituents with respect to the total initial dry solid weights excluding CaCl$_2$. For comparison, a series of zeolite−CNF films were also prepared without any addition of CaCl$_2$ and PEG. Free standing ZSM-5−CNF films with different ZSM-5 to CNF ratios were prepared by using 0.1, 0.5, 0.9, and 2 wt % aqueous ZSM-5 dispersion. The resulting ZSM-5−CNF films after drying had a zeolite content of 60, 89, 94, and 97 w/w%, respectively. The composition of the zeolite−CNF films are sometimes reported based on volume fraction of CNF, see Tables S1 and S2 in the Supporting Information.

Characterization. Field emission gun scanning electron microscope (FEG-SEM, JSM-700F, JEOL, JAPAN) with a working distance of 6 mm and accelerating voltage of 1.5 kV was used. The surface areas were calculated by the Brunauer Emmet and Teller (BET) model using the N$_2$ uptake collected on an ASAP 2020 analyzer (Micromeritics, Norcross GA, USA) within a 0.05−0.15 P/P_0 relative pressure range. The as-received powders were degassed under vacuum at 300 °C for 10 h before the N$_2$ adsorption measurements. The zeolite−CNF films were degassed under vacuum at 80 °C for 5 h. This treatment is not sufficient to remove all water in the films but higher temperatures were not used to avoid cellulose degradation. Infrared (IR) spectroscopy was performed using an FTIR spectrometer (Varian 670, Varian, Inc., USA) equipped with an attenuated total reflection (ATR, single reflection diamond element) and detection device (Goldengate by Specac). One hundred scans were accumulated in the spectral region of 390−4000 cm^{-1} with a spectral resolution of 4 cm^{-1}. Thermogravimetric analysis (TGA7, PerkinElmer, USA) was used to measure the amount of water and thiols adsorbed on the zeolite powders. The temperature was increased at a rate of 20 °C/min from room temperature to 900 °C under a flow of dry air. The maximum thiol uptake was determined by exposing zeolite powders (20 mg) in a sealed polyethylene tube containing 100 μL of liquid thiols at the boiling temperature of the thiols for 1 h. The zeolite powders were removed from the tube and exposed to air for 1 h to remove loosely attached thiols prior to TGA measurements. The difference between the total weight loss of zeolites at 900 °C after and before exposure to thiols is reported as the amount of thiols adsorbed on each respective zeolite powder after subtracting the weight loss due to water evaporation.

Quantitative solid-phase microextraction (SPME) followed by gas chromatography/mass spectrometry (GC/MS) analysis was used to determine the thiol vapor concentration in a sampling container. The GC/MS equipment used was a Varian CP-3800 gas chromatograph connected to a Varian 4000 ion trap mass spectrometer (Varian Inc., Walnut Creek, CA). The SPME fiber used was coated with an 85-μm carboxen/polydimethylsiloxane (CAR/PDMS) film with a high affinity

for polar volatile organic compounds (VOCs). The fiber was exposed to the thiol-containing vapor for 30 min at room temperature to ensure that equilibrium between vapor phase and fiber was achieved. The SPME fiber was extracted from the sampling container and inserted into the GC split/splitless injector (Varian 1177), where the gaseous material was desorbed at 150 °C in split-less mode for 5 min. The MS was operated in full scan mode within the m/z range 25−80 with electron ionization at 70 eV. The emission current was 25 μA, the number of μscans was 3 and the automatic gain control was set to 20000. The chromatographic peaks were integrated manually with the Varian MS data review software (version 6.9.3).

The mechanical strength of the zeolite−CNF films were measured by uniaxial tensile tests on an Instron 5944 with a load cell of 50 N. Prior to testing, the zeolite−CNF films were conditioned at 23 °C and a relative humidity of 50% for at least 2 days. The tensile tests were performed on rectangular films (35 mm by 5 mm) at 10% strain/min. Strain was calculated using digital image correlation (vic 2D and LIMESS) and the elastic modulus was calculated from the response in the linear region, typically between 0.1% and 0.3% strain.

Modeling and Computations. Modeling of the adsorption sites of the ethanethiol and propanethiol molecules in the respective adsorbents was investigated by geometry optimizations using periodic plane wave density functional theory (DFT) computations with periodic boundary conditions. The geometry optimization computations relax the system to the local minimum energy configuration. These simulations stabilize the adsorbate at the adsorption site enabling a prediction of the adsorption geometry and binding energy. The procedure is as follows: (1) A geometry optimization computation is performed on the framework structure returning the computed system energy E_{FW}. (2) The geometry of the adsorbate molecules is optimized and the system energy E_{thiol} is retrieved. (3) The optimized adsorbate coordinates are added to the coordinates of the optimized framework close to a hypothetical adsorption site (both at potential cation site and at the homogeneous SiO segment of the respective framework) and the geometry optimization is performed returning system energy $E_{FW+thiol}$. The heats of adsorption can then be estimated as follows:

$$\Delta H = E_{FW} + E_{thiol} - E_{FW+thiol}$$

Configurational biased grand canonical Monte Carlo (CB-GCMC) simulations were performed to calculate the thiol adsorption isotherms on three zeolites using the sorption module implemented in the Accelrys Materials Studio software suite.[34] The starting structures for both the adsorbates and the adsorbents were those previously optimized by the DFT and the interatomic forces are modeled by the universal type all-atom COMPASS force field.[35,36] The configuration bias allows the adsorbates to alternate the specified tetrahedral angles taking into account the rotational flexibility of the thiols. The interatomic distances of the adsorbates are however held fixed, as is the geometry of the adsorbents. The isotherms are simulated at 20 linearly scaled pressure points ranging up to 2.0 kPa at 298 K. At each pressure point the simulation was first run for 1×10^6 to equilibrate the system, followed by another 1×10^7 simulation steps providing the data from which the results were averaged. To get an indication on how the presence of water affects the uptake, the adsorption isotherms were simulated for each adsorbent−adsorbate combination both with and without water molecules present in the structure. The water molecules were loaded prior to the CB-GCMC simulations being performed using a simulated annealing algorithm. During the CB-GCMC simulations the water molecules were, geometrically, held fixed in the framework. The amount of water loaded into each structure corresponded to the respective water content measured by TGA. It should be noted that these CB-GCMC simulations treat the water molecules as a rigid part of the structure, which gives an uncertain amount of bias, as the water-thiol adsorption is likely to be more or less competitive. Hence, these simulations should be seen comparatively rather than absolute values. For a more elaborate and informative investigation of the effect of water on the adsorbent−adsorbate interactions, system dynamics should be taken
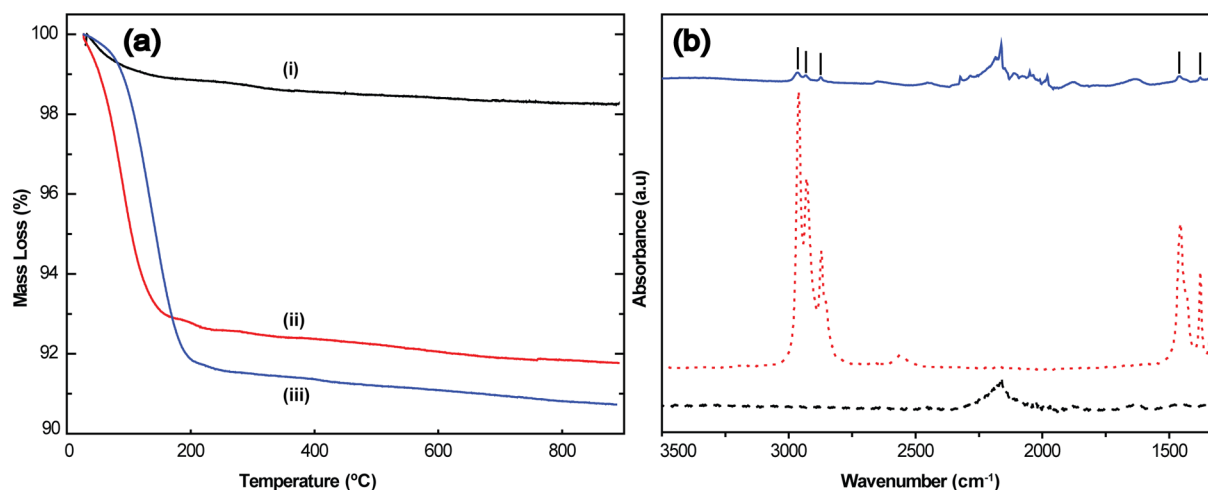
Figure 2. Uptake and interactions of thiols with ZSM-5. (a) Thermogravimetric (TG) curves of ZSM-5 powders: (i) as received, (ii) after exposure to ethanethiol for 1 h, and (iii) after exposure to propanethiol for 1 h. (b) Infrared spectra of as received ZSM-5 powder (dashed line), propanethiol (dotted line), and ZSM-5 powder after 1 h exposure to propanethiol (solid line). The C−H stretching vibrations at 2875, 2930, and 2965 cm^{-1} and C−H deformation vibrations at 1375 and 1455 cm-1 typical for propanethiol are indicated with vertical lines. The powders were not degassed before exposure to the thiols.

into account and an electron-level model would be preferred, such as DFT-based molecular dynamics methods.

RESULTS AND DISCUSSION

The thiol uptake of the zeolite powders could be estimated from the difference in mass loss of the zeolite powder, for example, ZSM-5 after exposure to thiols (Figure 2aii and 2aiii) compared with the mass loss of the unexposed ZSM-5 powder (Figure 2ai). The thiol uptake data given in Table 1 that was

Table 1. Water Content and Ethanethiol/Propanethiol Uptake Capacity of Zeolite Powders Determined by TGA^a

	zeolite			
adsorbate	ZSM-5 (mg/g)	silicalite-1 (mg/g)	zeolite beta (mg/g)	mordenite (mg/g)
water	17	16	120	83
ethanethiol	57 (100)	44 (100)	15	18
propanethiol	83 (110)	74 (110)	15	27

^{a}The zeolite powders were not degassed before exposure to the thiols for TGA measurement. The uptake values in parentheses are obtained from simulated thiol adsorption isotherms in the presence of water.

obtained from TGA data of the mass loss (Figure S1 in the Supporting Information) shows that ZSM-5 and silicalite-1 display the highest thiol uptake capacity. The adsorption of thiols on zeolite beta and mordenite is insignificant, which probably is related to their high water uptake. The TGA study thus suggests that zeolites of the MFI type (ZSM-5, silicalite-1) are suitable adsorbents of thiols also in the presence of moisture.

Figure 2b shows that IR bands characteristic for C−H stretching of thiols at 2875, 2930, and 2965 cm^{-1} and C−H bending vibrations at 1375 and 1455 cm^{-1}, appear after exposure of ZSM-5 to the thiols (Figure 2b), thus corroborating the significant uptake of thiols by ZSM-5 shown by TGA.

Adsorption isotherms of ethanethiol and propanethiol for silicalite-1 and ZSM-5 (Figure 3a and b), have also been calculated using the Configurational Biased Grand Canonical Monte Carlo (CB-GCMC) algorithm.[37] The CB-GCMC simulations suggest that the uptake capacity of thiols is only increased by about 20% in water-free zeolites (Figure 3b) compared to the water-containing zeolites (Figure 3a). This is related to the high surface area of MFI framework, S_{BET} = 400 m^2/g (Figure S2 in Supporting Information) that is only
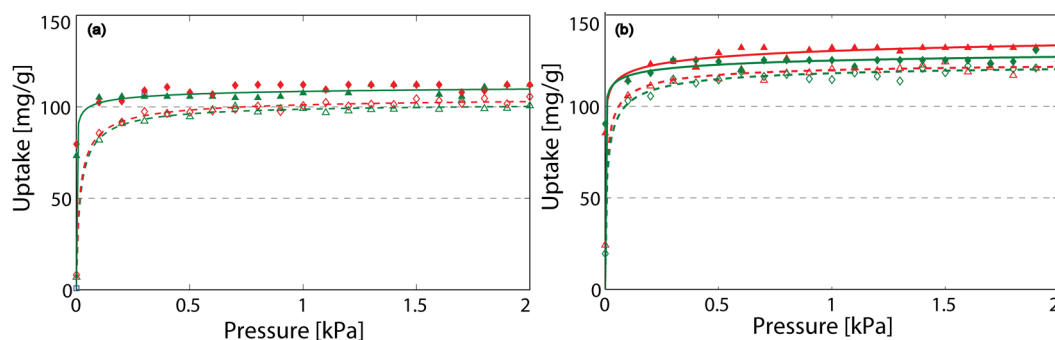

Figure 3. CB-GCMC simulated adsorption isotherms for ethanethiol and propanethiol on zeolitic frameworks (silicalite-1 (triangles); ZSM-5 (diamonds) that (a) contain water and (b) are dry. The markers show the simulated data points while the lines are the fitted Toth model isotherms. The ethanethiol isotherms have dashed lines and open markers and the propanethiol isotherms have solid lines and filled markers.

slightly reduced by the presence of water (Figure S2 in Supporting Information). Table 1 show that the simulated ethanethiol uptake capacity of silicalite-1 and ZSM-5 are almost twice of the uptake capacity obtained by TGA analysis on water-containing zeolites. The simulated propanethiol adsorption on silicalite-1 and ZSM-5 is up to 30% higher than the values obtained from TGA data on water-containing zeolites. Hence, the simulated thiol adsorption data confirm the TGA measurements that ZSM-5 (MFI) and silicalite-1 (MFI) have a high affinity and uptake capacity for thiols, also in the presence of water.[38]

The heats of adsorption calculated by DFT (Table 2) show that the thiols interact significantly stronger at the cation sites

Table 2. DFT Computed Heats of Adsorption for Ethanethiol and Propanethiol in FAU and MFI Frameworks at the SiO Site and the Respective Cation Sites

	adsorbent	
adsorbate	MFI/SiO site (kJ/mol)	MFI/NH_4^+ site (kJ/mol)
ethanethiol	74.5	111
propanethiol	88.4	124

than at the homogeneous SiO framework sections of zeolites. This is indicated by a 30% and 50% increase in the heats of adsorption computed respectively for cation-containing MFI (NH_4^+−ZSM-5) frameworks compared with their noncationic sites (Table 2). The DFT geometry optimization at cation sites (Figure 4a) shows how the nonbonding pair electron of the sulfur atom in the ethanethiol molecule contributes to the formation of a strong hydrogen bond with the hydrogen atoms of NH_4^+ in ZSM-5.[39] Indeed, the bonds between sulfur and H^+ in NH_4^+−ZSM-5 (2.1 Å) are the shortest bonds formed in the cavity. The heat of adsorption of propanethiol on homogeneous SiO framework of zeolites is higher than the heat of adsorption of ethanethiol by 16% for MFI frameworks (Table 2). The main reason for this difference is the higher interaction area of the larger molecule of propanethiol compared to ethanethiol; that is, the molecules that contain more hydrogen atoms (Figure 4b) adsorb more strongly. However, despite of higher heats of adsorption of propanethiol compared with ethanethiol (Table 2), the TGA data (Table 1) and the simulated isotherms (Figure 3) indicate that ethanethiol and propanethiol are adsorbed with approximately similar quantities.

The DFT data in Table 2 shows that MFI (SiO) framework has a high affinity to thiols, with substantial heats of adsorption. In a small pore zeolite, such as MFI type, the thiols fill out the pore effectively and the nonpolar hydrocarbon tail of the thiols can thus interact through short-range van der Waals forces with the O atoms of the MFI-pore. This results in strong interactions with the framework in total and hence high heats of adsorption. This trend has for example been shown experimentally and discussed by Savitz et al., where heats of adsorption were measured for alkanes in high silica zeolites with different pore diameters.[40] Hence, the modeling suggests that thiols also at low pressure should have a high affinity to the MFI framework.

In summary, the simulations and experimental studies have shown that ZSM-5 and silicalite-1 are suitable adsorbents for removal of the thiols of interest. These zeolites have thus been selected for the preparation of functional composite films and we have evaluated their mechanical properties and removal performance. A film composed of zeolite Y was also prepared for comparison of the mechanical properties. Free standing films of the zeolite powders together with cellulose nanofibrils (CNF, Figure S3 Supporting Information) have been prepared by colloidal processing[41,42] involving mixing and homogenization of a stable colloidal dispersion, gelation by Ca-ions, and water removal by vacuum filtration (Figure 1). Electrokinetic measurements of the zeolite dispersions after deagglomeration (Table 3) show that the particles are negatively charged with a

Table 3. Zeta Potential and pH of Zeolite, Cellulose Nanofibrils, and Zeolite−CNF Dispersions

zeolite type	ζ potential (mV)		pH of dispersions	
	as received	zeolite + $CaCl_2$	zeolite	zeolite + $CaCl_2$ + PEG + CNF
silicalite-1	−45	−30	6.0	6.0
ZSM-5	−40	−27	6.0	6.0
zeolite Y	−40	−20	4.0	4.0
CNF	−40			

zeta potential between −40 and −45 mV, which is sufficient to create an electrostatically stabilized dispersions. Addition of calcium ions (13 mmol/L) to the zeolite dispersion decrease the magnitude of the zeta potential from about −45 to −30 mV, but the stability of the dispersion is maintained and the pH of the dispersion is not affected (Table 3). Further addition of small quantities of polyethylene glycol (PEG) to the zeolite
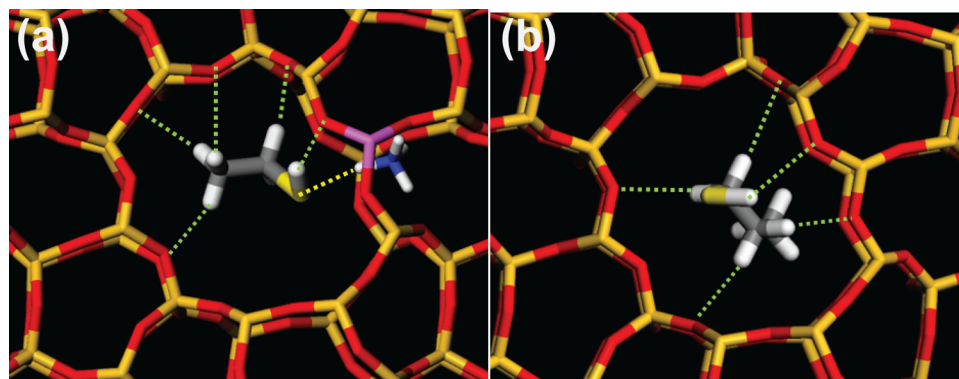

Figure 4. DFT geometry optimizations for (a) ethanethiol in MFI cation site (NH_4^+−ZSM5) and (b) propanethiol in MFI at noncation interacting adsorption sites.

dispersion does not affect the colloidal stability. When cellulose was added to zeolite dispersion, large agglomerates of zeolite–CNF particles that were interconnected to each other were formed and were visible to the naked eye. Previous work has shown that addition of calcium ions to negatively charged CNF results in the formation of strong hydrogels.[43,44] SEM micrographs of a freeze-dried dispersion of zeolite–CNF (Figure S4, Supporting Information) showed that a three-dimensional network of zeolite particles and CNF is already formed in the dispersion after mixing.

Figure 5 shows examples of the resulting free-standing and flexible zeolite–CNF films with a thickness of about 100–120
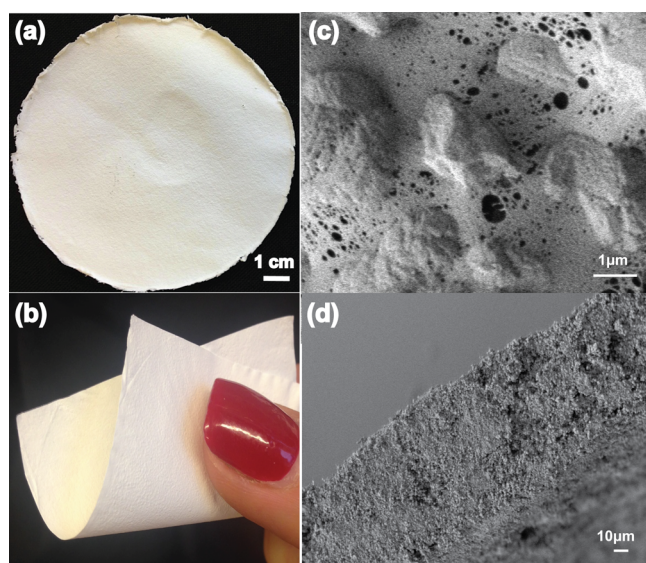

Figure 5. Free-standing zeolite–CNF films: (a) Photograph of zeolite–CNF free-standing films with a zeolite content of 89 w/w% after drying; (b) demonstration of the flexibility of zeolite–CNF films; (c) SEM micrograph of ZSM-5–CNF top surface zeolite particles entrapped and connected by cellulose network; and (d) SEM cross sectional view of ZSM-5–CNF film with a relatively uniform thickness of 100–120 μm.

μm after drying at 30 °C and 50% relative humidity for 24 h. The TGA curves in Figure S5, Supporting Information suggests that some water (less than 3 wt %) remains in the zeolite–CNF films prepared with ZSM-5 and silicalite-1 after drying. SEM micrograph of the ZSM-5–CNF (Figure 5c) shows that the ZSM-5 zeolite particles are homogeneously distributed in the CNF network.

Figure 6 shows that the tensile strength of the composite ZSM-5–CNF films reaches values of 8 MPa and higher when the CNF content is above 6 vol %. The tensile strength is substantially reduced at lower CNF content and at a CNF content of about 3 vol % (Figure 6, Supporting Information Table S1), the mechanical integrity is essentially lost. This suggests that the strength and flexibility is primarily determined by the CNF network and that the CNF content has to be sufficiently high to enable the nanosized fibrils to form a percolating network.[45] The strength of three different zeolite–CNF films prepared with CNF content of 10 vol % decreases in the following order: ZSM-5–CNF > silicalite-1–CNF > zeolite Y–CNF (Figure 6a). Table 4 shows that this order has an inverse correlation to the porosity of the films. The least porous films were obtained with the spherical ZSM-5 particles (63% porosity) while the irregularly shaped zeolite powders in silicalite-1–CNF and zeolite Y–CNF films have a higher porosity, 65% and 70%, respectively. The stress–strain curves of the zeolite–CNF films (Figure 6b) follow the characteristic features of a neat CNF film (nanopaper) where the initial elastic response is followed by yielding and strain hardening.[31] The film with ZSM-5 shows the highest modulus, yield strength and ultimate strength (Table 4). Plastic deformation in the composites increases strain to failure beyond the yield point (Table 4 and Figure 6). The films with zeolite Y and silicalite-1 have similar yield strength (Figure 6b). Further investigations showed that the presence of Ca^{2+} and PEG did not have a significant effect on the mechanical properties of dry zeolite–CNF films and similar values of modulus and strength were obtained as for the films containing Ca^{2+} and PEG (Table S3, Supporting Information). Hence, the mechanical measurements strongly suggest that it is the CNF network that controls the mechanical properties, and because CNF is such a strong
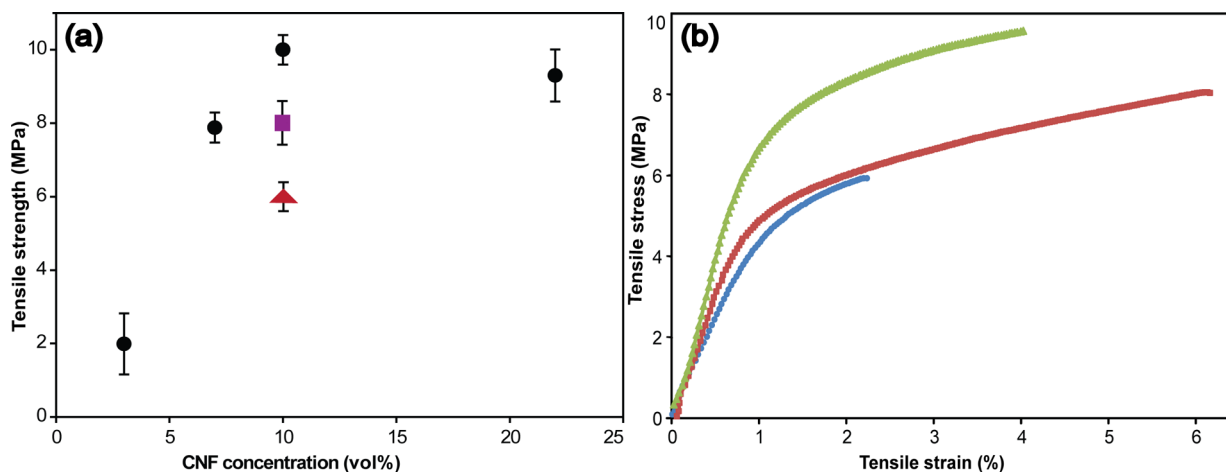

Figure 6. Mechanical properties of zeolite–CNF films. (a) Tensile strength of ZSM-5–CNF films at different amount of CNF in the film (circles), and strength of films containing 10 vol % of CNF with silicalite-1 (square) and zeolite Y (triangle). (b) Tensile stress as a function of tensile strain for zeolite–CNF films containing 10 vol % of CNF: ZSM-5–CNF (green triangles), silicalite-1–CNF (red squares), and zeolite Y–CNF (blue circles).

Table 4. Textural and Mechanical Properties of ZSM-5−CNF, Zeolite Y-CNF, and Silicalite-1-CNF Films Containing 89 w/w% Zeolites Together with Ca^{2+}-Ions and PEG^{a}

composite	zeolite particle size (μm)	BET surface areas (m^2 g)	micropore volume (cm^3 g)	porosity (vol %)	Young's modulus (GPa)	tensile strength (MPa)	strain to failure (%)
ZSM-5−CNF	0.5−1.5	240	0.08	63.0	1.1 (0.1)	10 (0.4)	4.09 (0.5)
zeolite Y−CNF	0.5−1.5	560	0.16	70.0	0.5 (0.1)	6.0 (0.1)	2.05 (0.3)
silicalite-1−CNF	3.0−5.0	180	0.06	65.0	0.7 (0.1)	8.0 (0.6)	6.23(1.0)

^{a}BET surface area and micropore volume are calculated from N$_2$ adsorption and t-plot, respectively. Theoretical porosities are calculated based on experimental density of the films (Appendix A, Supporting Information). The values of standard deviations are given in parentheses.
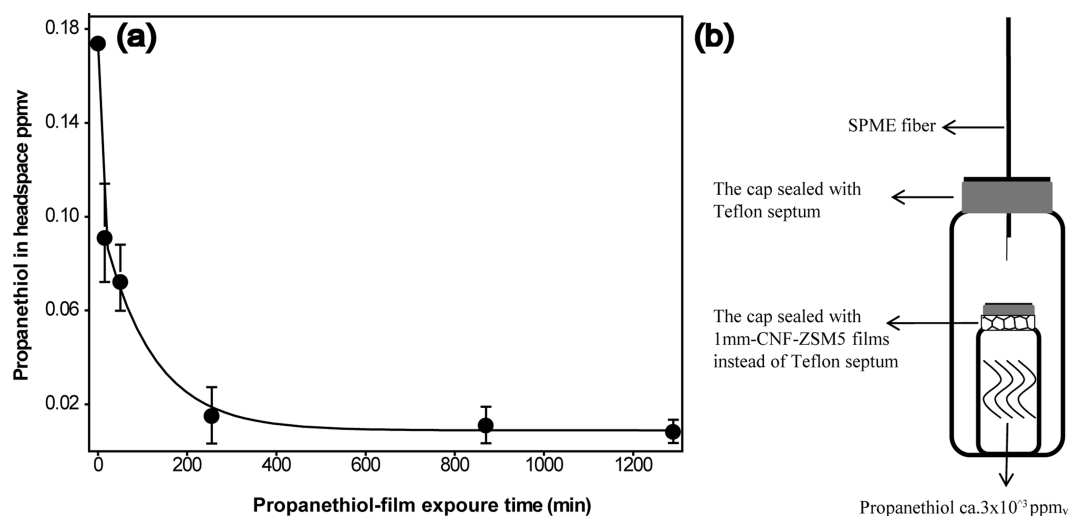

Figure 7. Thiol elimination from the head space of a container: (a) Decrease of the propanethiol vapor concentration with time after adding 0.35 g of a ZSM-5−CNF film to the sampling container; (b) Schematic presentation of the test measuring the propanethiol outflow through 1 mm ZSM-5−CNF films.

material,[31] it is possible to produce strong films also at a zeolite content at 90 w/w% and above.

Manual bending of the films showed that the flexibility is improved when Ca^{2+} and PEG are present. In bending, the films are subjected to both tension and compression. The reason may therefore be that the friction and bonding between the inorganic particles and the CNF network is influenced by the presence of Ca^{2+} and PEG, resulting in a better flexibility and reduced brittleness. The BET surface area of zeolite−CNF films obtained by nitrogen adsorption was high, for example, 560 m^2/g for zeolite Y−CNF film (Supporting Information Figure S1), even though some water remained in the films after the mild pretreatment in vacuum at 80 °C and 5 h. It should be noted that the BET surface area of the zeolite−CNF films were only reduced by about 20% compared with the as received zeolite powders (Supporting Information Figure S1), showing that the preparation of CNF-based composite films did not result in significant pore blockage.

Thiols are very potent odors and already concentrations on the part-per-million-level can be unbearable to the human olfactory system. Indeed, the concentration of thiols within the headspace of packages of certain vegetables or fruits can reach these levels after prolonged storage.[46,47] Hence, there is a need to develop odor eliminating solutions that can be integrated with commercial packaging materials. In the present work, we have investigated the propanethiol removal capacity of zeolite−CNF films at vapor concentrations around 1 ppm$_v$ and below using SPME/GC/MS. To produce a standard vapor concentration at 0.2 ppm$_v$, a volume of 0.02 μL of propanethiol was

injected into a 30-L container, sealed with a Teflon septum and allowed to equilibrate. SPME and GC/MS analysis at different time intervals showed an unchanged thiol concentration with no detectable losses up to 24 h after injection (longer periods of time were not investigated). Placing a small CNF-zeolite film (0.35 g) into the container resulted in a decrease of the thiol concentration to a level as low as 0.009 (±0.005) ppm$_v$, (Figure 7a). The uptake progresses with time and Figure 7a shows the decrease in thiol concentration with times. Exposure times beyond 20 h did not yield any further significant reduction in thiol level (Figure 7). A simple sniff test performed by four different persons after allowing the CNF-zeolite film to deodorize the thiol vapor in the container, indicates that the ZSM-5−CNF film is able to reduce the propanethiol concentration down to levels where it is not clearly detected by the human olfactory system, and thus of minor or no discomfort. A control test showed that a pure CNF film cross-linked by calcium ions does not reduce the thiol concentration in the container. Hence, the CNF is not contributing to the adsorption process.

The ability of a 1 mm thick ZSM-5−CNF film (10 compressed layers) to serve as a membrane for propanethiol vapor at high concentration (∼3 × 10^3 ppm$_v$) was investigated by the setup shown in Figure 7b. Sampling of the gas outside the propanethiol-filled cylinder with SPME and GC/MS analysis, showed no detectable propanethiol and thus a complete elimination by the ZSM-5−CNF film (Supporting Information Figure S6b). The combination of fast uptake rates

and good sealing properties offers a potential application of zeolite−CNF films in the packaging industry.

CONCLUSIONS

Zeolites of MFI-type, ZSM-5, and silicalite-1 were identified as highly efficient adsorbents for adsorption of light thiols, for example, ethanethiol and propanethiol. Functional and flexible free-standing zeolite−CNF films with content of active zeolite of around 90 wt % and a thickness of 100−120 μm were achieved through colloidal processing involving vacuum filtration and Ca-ion cross-linking. The free-standing films of zeolite−CNF fabricated in this work combine high mechanical strength of about 10 MPa with high bending flexibility. We found that the network of the very strong CNF control the mechanical properties of the composite films and CNF content as low as 6 vol % is sufficient to produce a strong film. Headspace gas chromatography measurements and sniff test demonstrated that zeolite−CNF films can remove thiols below the human olfactory threshold when exposed to low thiol concentrations <0.2 ppm. A combination of high thiol removal performance and mechanical stability suggest zeolite−CNF composites as a potential candidate for use in active packaging material where the package contents, for example, fruits, foods, and vegetables release considerable concentrations of odors.

ASSOCIATED CONTENT

ⓢ Supporting Information

Uptake of thiols by zeolites, nitrogen adsorption-desorption isotherms, picture of cellulose nanofibrils, SEM micrographs of freeze-dried ZSM5-CNF dispersion, TGA curves of the three zeolite−cellulose nanofibril films, headspace SPME/GC/MS analyses, weight and volume (%) fractions of each component, physical properties of zeolite−CNF films, and Appendix A. The Supporting Information is available free of charge on the ACS Publications website at DOI: 10.1021/acsami.5b02252.

AUTHOR INFORMATION

Corresponding Author

*Phone: +46-8-162368. E-mail: Lennart.Bergstrom@mmk.su.se.

Notes

The authors declare no competing financial interest.

ACKNOWLEDGMENTS

REFERENCES

(1) Alif, M. F.; Matsumoto, K.; Kitagawa, K. On-line Mass Spectrometric Analysis of Sulfur Compounds in Hydrothermal Process of Durian and Vegetables. *Microchem. J.* 2012, 103, 179−184.

(2) Carson, J. F. Chemistry and Biological Properties of Onions and Garlic. *Food. Rev. Int.* 1987, 3, 71−103.

(3) Nielsen, G. S.; Poll, L. Determination of Odor Active Aroma Compounds in Freshly Cut Leek (*Allium ampeloprasum* Var. *Bulga*) and in Long-Term Stored Frozen Unblanched and Blanched Leek Slices by Gas Chromatography Olfactometry Analysis. *J. Agric. Food Chem.* 2004, 52, 1642−1646.

(4) Chin, S. T.; Nazimah, S. A. H.; Quek, S. Y.; Che Man, Y. B.; Abdul Rahman, R.; Mat Hashim, D. Analysis of Volatile Compounds from Malaysian Durians (*Durio zibethinus*) Using Headspace SPME Coupled to Fast GC-MS. *J. Food Compos. Anal.* 2007, 20, 31−44.

(5) Näf, R.; Velluz, A. Sulphur Compounds and Some Uncommon Esters in Durian (*Durio zibethinus Murr*). *Flavour Fragrance. J.* 1996, 11, 295−303.

(6) Jo, W. K.; Shin, S. H.; Hwang, E. S. Removal of Dimethyl Sulfide Utilizing Activated Carbon Fiber-Supported Photocatalyst in Continuous-Flow System. *J. Hazard. Mater.* 2011, 191, 234−9.

(7) Ding, L.; Liu, T. X.; Li, X. Z. Removal of CH$_3$SH With In-Situ Generated Ferrate (VI) in a Wet-Scrubbing Reactor. *J. Chem. Technol. Biotechnol.* 2014, 89, 455−461.

(8) Hwang, C. L.; Tai, N. H. Removal of Dimethylsulfide by Adsorption on Ion-Exchanged Zeolites. *Appl. Catal., B* 2010, 93, 363−367.

(9) Weber, G.; Benoit, F.; Bellat, J. P.; Paulin, C.; Mougin, P.; Thomas, M. Selective Adsorption of Ethyl Mercaptan on NaX Zeolite. *Microporous Mesoporous Mater.* 2008, 109, 184−192.

(10) Wang, X. L.; Fan, H. L.; Tian, Z.; He, E. Y.; Li, Y.; Shangguan, J. Adsorptive Removal of Sulfur Compounds Using IRMOF-3 at Ambient Temperature. *Appl. Surf. Sci.* 2014, 289, 107−113.

(11) Urlaub, J. J.; MacDonald, J. G. High Surface Area Material Blends For Odor Reduction, Articles Utilizing Such Blends and Methods of Using Same. U.S. Patent 8,211,369, June 4, 2012.

(12) Arehart, K. D.; Aschenbrenner, F.; Monta, A. G. D. Odor Control Cellulose-Based Granules. U.S. Patent 8,158,155, April 17, 2012.

(13) Howard, F. Laminated Paper Containing Activated Carbon. U.S. Patent 2,593,146, April 15, 1952.

(14) Blinka, T. A.; Edwards, F. B.; Miranda, N. R.; Speer, D. V.; Thomas, J. A. Zeolite in Packaging Film. U.S. Patent 5,834,079, November 10, 1998.

(15) Gioffre, A.; Marcus, B. K. Process for Eliminating Organic Odors and Compositions For Use Therein. U.S. Patent 4,795,482, January 3, 1989.

(16) Huang, Z.; Guo, Y. H.; Zhang, T. M.; Zhang, X. H.; Guo, L. Y. Fabrication and Characterization of Zeolite Beta-filled Polyethylene Composite Films. *Packag. Technol. Sci.* 2012, 26, 1−10.

(17) Fujimoto, Y.; Nakano, M.; Sugiyama, K.; Utsunomiya, T. Composition Containing a Zeolite−Cellulose Composite and Product Made Therefrom. E.P. 0,938,925, August 31, 2005.

(18) Davis, M. E. Zeolites and Molecular Sieves: Not Just Ordinary Catalysts. *Ind. Eng. Chem. Res.* 1991, 30, 1675−1683.

(19) Dyer, A. Separation of Closely Related Systems by Molecular Sieve Zeolites. *Sep. Sci. Technol.* 1978, 13, 501−516.

(20) Yi, D.; Huang, H.; Meng, X.; Shi, L. Adsorption−Desorption Behavior and Mechanism of Dimethyl Disulfide in Liquid Hydrocarbon Streams on Modified Y Zeolites. *Appl. Catal., B* 2014, 148−149, 377−386.

(21) Satokawa, S.; Kobayashi, Y.; Fujiki, H. Adsorptive Removal of Dimethylsulfide and T-butylmercaptan From Pipeline Natural Gas Fuel on Ag Zeolites Under Ambient Conditions. *Appl. Catal., B* 2005, 56, 51−56.

(22) Cammarano, C.; Huguet, E.; Cadours, R.; Leroi, C.; Coq, B.; Hulea, V. Selective Transformation of Methyl and Ethyl Mercaptans Mixture to Hydrocarbons and H$_2$S on Solid Acid Catalysts. *Appl. Catal., B* 2014, 156−157, 128−133.

(23) Khan, N. A.; Jhung, S. H. Low-Temperature Loading of Cu$^+$ Species Over Porous Metal-Organic Frameworks (MOFs) and Adsorptive Desulfurization With Cu$^+$-Loaded MOFs. *J. Hazard. Mater.* 2012, 237−238, 180−185.

(24) Foster, M. D.; Rivin, I.; Treacy, M. M. J.; Delgado Friedrichs, O. A Geometric Solution to The Largest Free Sphere Problem in Zeolite Frameworks. *Microporous Mesoporous Mater.* 2006, 90, 32−38.

(25) Larsen, G.; Vu, D.; Sanchez, M. M. A Stable Zeolite/Cellulose Composite Materials And Method of Preparation Therein. U.S. Patent 6,814,759, November 9, 2004.

(26) Li, Y.; Guan, H. M.; Chung, T. S.; Kulprathipanja, S. Effects of Novel Silane Modification of Zeolite Surface on Polymer Chain Rigidification and Partial Pore Blockage in Polyethersulfone (PES) Zeolite A Mixed Matrix Membranes. *J. Membr. Sci.* 2006, 275, 17−28.

(27) Moore, T. T.; Mahajan, R.; Vu, D. Q.; Koros, W. J. Hybrid Membrane Materials Comprising Organic Polymers With Rigid Dispersed Phases. *AIChE. J.* **2004**, *50*, 311−321.

(28) Aroon, M. A.; Ismail, A. F.; Matsuura, T.; Montazer Rahmati, M. M. Performance Studies of Mixed Matrix Membranes For Gas Separation: A Review. *Sep. Purif. Technol.* **2010**, *75*, 229−242.

(29) Aulin, C.; Salazar-Alvarez, G.; Lindstrom, T. High Strength, Flexible and Transparent Nanofibrillated Cellulose-Nanoclay Biohybrid Films With Tunable Oxygen and Water Vapor Permeability. *Nanoscale* **2012**, *4*, 6622−6628.

(30) Isogai, A.; Saito, T.; Fukuzumi, H. TEMPO-Oxidized Cellulose Nanofibers. *Nanoscale* **2011**, *3*, 71−85.

(31) Henriksson, M.; Berglund, L.; Isaksson, P.; Lindström, T.; Nishino, T. Cellulose Nanopaper Structures of High Toughness. *Biomacromolecules* **2008**, *9*, 1579−1585.

(32) Saito, T.; Hirota, M.; Tamura, N.; Kimura, S.; Fukuzumi, H.; Heux, L.; Isogal, A. Individualization of Nano-Sized Plant Cellulose Fibrils by Direct Surface Carboxylation Using TEMPO Catalyst Under Neutral Conditions. *Biomacromolecules* **2009**, *10*, 1992−1996.

(33) Liu, A.; Walther, A.; Ikkala, O.; Belova, L.; Berglund, L. A. Clay Nanopaper With Tough Cellulose Nanofiber Matrix for Fire Retardancy and Gas Barrier Functions. *Biomacromolecules* **2011**, *12*, 633−641.

(34) Use Accelrys Materials Studio for materials modeling and simulation. http://accelrys.com/products/materials-studio (accessed Oct 20, 2014).

(35) Sun, H. COMPASS: An AB Initio Force-Field Optimized For Condensed-Phase Applications Overview With Details on Alkane and Benzene Compounds. *J. Phys. Chem. B* **1998**, *102*, 7338−7364.

(36) Zhao, L.; Liu, L.; Sun, H. Semi-ionic Model for Metal Oxides and Their Interfaces with Organic Molecules. *J. Phys. Chem. C* **2007**, *111*, 10610−10617.

(37) Siepmann, J. I.; Frenkel, D. Configurational Bias Monte Carlo: A New Sampling Scheme For Flexible Chains. *Mol. Phys.* **1992**, *75*, 59−70.

(38) Ju, S. G.; Zeng, Y. P.; Yao, H. Q. Computer Simulation of The Adsorption of Ethanethiol in Silicalite of MFI and MOR. *J. Chem. Phys.* **2004**, *121*, 9098−9102.

(39) Soscún, H.; Castellano, O.; Hernandez, J.; Arrieta, F.; Bermúdez, Y.; Hinchliffe, A.; Brussin, M. R.; Sanchez, M.; Sierraalta, A.; Ruette, F. An AB Initio and DFT Study of The Interaction Between Ethanethiol and Zeolites. *J. Mol. Catal. A: Chem.* **2007**, *278*, 165−172.

(40) Savitz, S.; Siperstein, F.; Gorte, R. J.; Myers, A. L. Calorimetric Study of Adsorption of Alkanes in High-Silica Zeolites. *J. Phys. Chem. B* **1998**, *102*, 6865−6872.

(41) Andersson, N.; Alberius, P.; Ortegren, J.; Lindgren, M.; Bergström, L. Photochromic Mesostructured Silica Pigments Dispersed in Latex Films. *J. Mater. Chem.* **2005**, *15*, 3507−3513.

(42) Lagerwall, J. P. F.; Schütz, C.; Salajkova, M.; Noh, J. H.; Park, J. H.; Scalia, G.; Bergström, L. Cellulose Nanocrystal-Based Materials: From Liquid Crystal Self-assembly And Glass Formation to Multifunctional Thin Films. *NPG Asia Mater.* **2014**, *6*, No. e80, DOI: 10.1038/am.2013.69.

(43) Dong, H.; Snyder, J. F.; Williams, K. S.; Andzelm, J. W. Cation-Induced Hydrogels of Cellulose Nanofibrils with Tunable Moduli. *Biomacromolecules.* **2013**, *14*, 3338−3345.

(44) Zander, N. E.; Dong, H.; Steele, J.; Grant, J. T. Metal Cation Cross-Linked Nanocellulose Hydrogels as Tissue Engineering Substrates. *ACS Appl. Mater. Interfaces.* **2014**, *6*, 18502−18510.

(45) Favier, V.; Chanzy, H.; Cavaille, J. Y. Polymer Nanocomposites Reinforced by Cellulose Whiskers. *Macromolecules* **1995**, *28*, 6365−6367.

(46) Forney, C. F.; Mattheis, J. P.; Austin, R. K. Volatile Compounds Produced by Broccoli Under Anaerobic Conditions. *J. Agric. Food Chem.* **1991**, *39*, 2257−2259.

(47) Hansen, M.; Buttery, R. G.; Stern, D. J.; Cantwell, M. I.; Ling, L. C. Broccoli Storage Under Low-Oxygen Atmosphere: Identification of Higher Boiling Volatiles. *J. Agric. Food Chem.* **1992**, *40*, 850−852.